Computers and Structures 212 (2019) 299–310

Contents lists available at ScienceDirect

Computers and Structures

journal homepage: www.elsevier.com/locate/compstruc

The Bathe time integration method with controllable spectral radius: The ρ_∞-Bathe method

Gunwoo Noh [a], Klaus-Jürgen Bathe [b,*]

[a] Kyungpook National University, Daegu 41566, Republic of Korea
[b] Massachusetts Institute of Technology, Cambridge, MA 02139, USA

ARTICLE INFO

Article history:
Received 14 October 2018
Accepted 5 November 2018

Keywords:
Transient analyses
Direct time integrations
Implicit and explicit schemes
Stability and accuracy
Bathe method
Dissipation and dispersion

ABSTRACT

We consider the Bathe implicit time integration method and focus on the time step splitting ratio and the spectral radius at large time steps to improve and generalize the scheme. The objective is to be able to prescribe the amplitude decay (dissipation) and period elongation (dispersion) for the numerical integration, and to achieve this aim in a direct and optimum manner with the minimum number of parameters. We show that the use of the time step splitting ratio and spectral radius is effective to prescribe in a smooth manner no amplitude decay to very large amplitude decays, with correspondingly small period elongation to very large period elongations while maintaining second-order accuracy. We analyze the effects of the splitting ratio and spectral radius on the stability and accuracy of the scheme and illustrate the use of these parameters in comparison with previously published methods. Furthermore, we show that with a proper setting of these parameters more accurate results may be obtained in some analyses.

1. Introduction

During the recent decades many direct time integration schemes for the solution of the time dependent finite element equations have been proposed and used. These integration schemes are employed for transient analyses of the dynamic response of structures and can be classified into explicit and implicit techniques [1]. The explicit schemes are mostly used for wave propagation solutions and the implicit methods are used for the analysis of short duration structural vibrations, but also in the solution of wave propagations. Since the schemes are very widely applied, it is important to pursue research for more understanding and more effective methods.

Some explicit schemes are the well-known central difference method [1,2] and those presented recently in Refs. [3–6]. In this paper we focus on an implicit time integration method, and in this category we have the Newmark scheme [7], the Houbolt method [8], the Wilson method [9,10], the methods proposed by Zhou and Tamma [11] and the three-parameter or generalized alpha scheme [12–14]. Since more recently, the Bathe method is increasingly used [15–17].

In the Bathe scheme, the time step is subdivided into two sub-steps. For the first sub-step the Newmark method of time integration is used and for the second sub-step the three-point Euler backward scheme is employed. While the method is thus a composite time integration scheme, it can also be thought of as a "single-step solve scheme" with certain computations performed within the step [18–20]. Other composite time integration schemes have since then also been proposed, see e.g. [21,22].

An advantage of the Bathe scheme is that while inherently three parameters are present (the Newmark δ, α values, and the time-step splitting ratio γ), these can be set to the default values $\delta = 0.5,\ \alpha = 0.25,\ \gamma = 0.5$, so that the trapezoidal rule is used in the first sub-step integration and the Euler method is employed with equal size sub-steps in the second sub-step integration. With this default setting, excellent accuracy is achieved in the solution of many problems, which is an advantage in engineering practice since it can be costly to experiment with different values of parameters for a time integration. This was an important point made in proposing this time integration scheme [16].

However, inherently the above parameters can be varied and it is natural to study the effect on stability and accuracy of using different values from the default values. In particular so, since analysts of other time integration schemes use parameters that are changed, see e.g. Ref. [14]. A study of the effects of changing these parameters in the Bathe method will also give more insight into the time integration scheme.

For these reasons, we studied the effects of changing the three parameters in the Bathe method in Refs. [19,20]. For unconditional

* Corresponding author.
E-mail address: kjb@mit.edu (K.J. Bathe).

https://doi.org/10.1016/j.compstruc.2018.11.001
0045-7949/

stability and optimal accuracy, the trapezoidal rule is best used for the first sub-step but, as shown in Ref. [20], the splitting ratio γ can take on values greater than 0, $\neq 1$, but even greater than 1. In this way, we can adjust the amplitude decay (dissipation) and period elongation (dispersion) by the use of different values of γ. However, the accuracy is not optimal, for example, when $\gamma = 0.99$ we have negligible amplitude decay but the period elongation is like when using the trapezoidal rule with the full time step. Hence the Bathe scheme is for this setting twice as expensive as the traditional trapezoidal rule.

Another way to proceed is to use $\gamma = 0.5$ and introduce new parameters that can be adjusted. This approach was pursued in Ref. [23], where the β_1/β_2-Bathe scheme was proposed. The basic idea in this approach is to use for the time integration over the second sub-step the Newmark approximation over the first and second sub-steps with the parameters β_1 and β_2, where these parameters act like the δ parameter in the Newmark approximation [1]. Using this scheme, the amplitude decay can be changed smoothly from zero to very large, and the period elongation changes correspondingly. In particular, when $\beta_1 = \beta_2 = 0.5$ the trapezoidal rule is used for each of the sub-steps, and when $\beta_1 = 1/3$ and $\beta_2 = 2/3$ the standard Bathe scheme (using $\gamma = 0.5$) is employed. These are good properties, however, the β_1/β_2-Bathe scheme requires the use of the two parameters β_1 and β_2 with the third parameter γ largely set to 0.5 for the analysis of properties in Ref. [23]. Of course, the effect of γ could be analyzed.

Another inherent parameter in the standard Bathe method is the spectral radius $\rho(\mathbf{A})$ of the amplification matrix $\mathbf{A}$ at very large values of $\Delta t/T$, where T is the free vibration period of the system, referred to as $\rho_\infty(\mathbf{A})$. In the standard Bathe scheme $\rho_\infty = 0.0$, and the fact that the spectral radius is equal to 1 for time steps Δt that satisfy $\Delta t/T \leqslant 0.3$ and then rapidly decreases to zero for larger time steps is a useful property [1]. This leads to accuracy in the frequencies to be integrated and the discarding of those frequencies from the response that cannot and should not be integrated because they are not excited or carry at most spurious response.

In order to reach a simple and effective scheme in which besides γ only one more parameter is employed, we have focused on the use of the standard Bathe method with the spectral radius ρ_∞ as an additional parameter. This research is thus a continuation of our work presented in Ref. [20].

In this paper we present this generalization of the Bathe method, in which we still use $\delta = 0.5,\ \alpha = 0.25$ for the first sub-step but we employ γ and ρ_∞ as parameters. The method is unconditionally stable, second-order accurate, and the amplitude decay and period elongation can be smoothly changed to have no amplitude decay, like when using the trapezoidal rule for both sub-steps, and very large amplitude decay, always with corresponding period elongations. Since we introduce ρ_∞ as an additional parameter in the standard Bathe scheme, we refer to the method as the ρ_∞-Bathe scheme. This method contains as special cases the standard Bathe scheme and, as we show below, also the β_1/β_2-Bathe scheme if the conditions of second-order accuracy are not imposed.

In the following sections, we present the basic time integration formulae of the ρ_∞-Bathe scheme, including the amplification matrix, and we discuss the properties of amplitude decay and period elongation when different sets of parameters (γ, ρ_∞) are used. We also evaluate the scheme in comparison to the use of the β_1/β_2 parameters in the Bathe method (with $\gamma = 0.5$) and in comparison to other methods, which provides novel insight. Based on this study, we conclude that the standard Bathe method with $\gamma = 0.5$ and $\rho_\infty = 0$ (of course, included in the ρ_∞-Bathe scheme) gives overall, in general, good accuracy but that the use of the parameters (γ, ρ_∞) can be valuable in the solution of some problems.

2. The ρ_∞-Bathe time integration scheme

Considering linear analysis, the governing finite element equations to be solved are

$$\mathbf{M}\ddot{\mathbf{U}} + \mathbf{C}\dot{\mathbf{U}} + \mathbf{K}\mathbf{U} = \mathbf{R} \tag{1}$$

with given initial conditions, where $\mathbf{M}$, $\mathbf{C}$, $\mathbf{K}$ are the mass, damping and stiffness matrices, and the vectors $\mathbf{U}$ and $\mathbf{R}$ list, respectively, the nodal displacements (rotations) and externally applied nodal forces (moments). An overdot denotes a time derivative. Assuming that the time step size Δt is set and all solution variables are known up to time t, the time integration scheme is to calculate the solution at time $t + \Delta t$.

In the Bathe method we calculate the unknown displacements, velocities, and accelerations at time $t + \Delta t$ by considering the time step Δt to consist of two sub-steps. The sub-step sizes are $\gamma\Delta t$ and $(1-\gamma)\Delta t$ for the first and second sub-steps, respectively.

In the first sub-step of the ρ_∞-Bathe scheme, as in the standard scheme, we use the trapezoidal rule for the equilibrium at time $t + \gamma\Delta t$,

$$\mathbf{M}\,{}^{t+\gamma\Delta t}\ddot{\mathbf{U}} + \mathbf{C}\,{}^{t+\gamma\Delta t}\dot{\mathbf{U}} + \mathbf{K}\,{}^{t+\gamma\Delta t}\mathbf{U} = {}^{t+\gamma\Delta t}\mathbf{R} \tag{2}$$

$${}^{t+\gamma\Delta t}\mathbf{U} = {}^{t}\mathbf{U} + \frac{\gamma\Delta t}{2}({}^{t}\dot{\mathbf{U}} + {}^{t+\gamma\Delta t}\dot{\mathbf{U}}) \tag{3}$$

$${}^{t+\gamma\Delta t}\dot{\mathbf{U}} = {}^{t}\dot{\mathbf{U}} + \frac{\gamma\Delta t}{2}({}^{t}\ddot{\mathbf{U}} + {}^{t+\gamma\Delta t}\ddot{\mathbf{U}}) \tag{4}$$

For the second sub-step, instead of using the 3-point Euler backward method as in the standard Bathe method, we use the following relations for the equilibrium at time $t + \Delta t$,

$$\mathbf{M}\,{}^{t+\Delta t}\ddot{\mathbf{U}} + \mathbf{C}\,{}^{t+\Delta t}\dot{\mathbf{U}} + \mathbf{K}\,{}^{t+\Delta t}\mathbf{U} = {}^{t+\Delta t}\mathbf{R} \tag{5}$$

$${}^{t+\Delta t}\mathbf{U} = {}^{t}\mathbf{U} + \Delta t(q_0\,{}^{t}\dot{\mathbf{U}} + q_1\,{}^{t+\gamma\Delta t}\dot{\mathbf{U}} + q_2\,{}^{t+\Delta t}\dot{\mathbf{U}}) \tag{6}$$

$${}^{t+\Delta t}\dot{\mathbf{U}} = {}^{t}\dot{\mathbf{U}} + \Delta t(s_0\,{}^{t}\ddot{\mathbf{U}} + s_1\,{}^{t+\gamma\Delta t}\ddot{\mathbf{U}} + s_2\,{}^{t+\Delta t}\ddot{\mathbf{U}}) \tag{7}$$

where $q_0, q_1, q_2, s_0, s_1, s_2$ and γ are parameters to be determined. We should note here that the Ansatz in Eqs. (6) and (7) is quite similar to the Ansatz used in Ref. [23] and with $s_0 = q_0 = \gamma(1-\beta_1)$, $s_1 = q_1 = \gamma(\beta_1 + \beta_2 - 1) + 1 - \beta_2$ and $s_2 = q_2 = (1-\gamma)\beta_2$, these time stepping relations reduce to the β_1/β_2-Bathe scheme. Table 1 summarizes already the various Bathe integration schemes. We discuss the similarities and the differences between the standard Bathe method, the β_1/β_2-Bathe scheme and the present method in Section 2.2.

Using the relations and the equilibrium equations in Eqs. (2)–(7), we can construct the time-stepping equations as

$$\hat{\mathbf{K}}_1\,{}^{t+\gamma\Delta t}\mathbf{U} = \hat{\mathbf{R}}_1 \tag{8}$$

$$\hat{\mathbf{K}}_2\,{}^{t+\Delta t}\mathbf{U} = \hat{\mathbf{R}}_2 \tag{9}$$

where

$$\hat{\mathbf{K}}_1 = \frac{4}{\gamma^2\Delta t^2}\mathbf{M} + \frac{2}{\gamma\Delta t}\mathbf{C} + \mathbf{K} \tag{10}$$

$$\hat{\mathbf{K}}_2 = \frac{1}{\Delta t^2 q_2 s_2}\mathbf{M} + \frac{1}{\Delta t q_2}\mathbf{C} + \mathbf{K} \tag{11}$$

$$\hat{\mathbf{R}}_1 = {}^{t+\gamma\Delta t}\mathbf{R} + \mathbf{M}\left({}^{t}\ddot{\mathbf{U}} + \frac{4}{\gamma\Delta t}{}^{t}\dot{\mathbf{U}} + \frac{4}{\gamma^2\Delta t^2}{}^{t}\mathbf{U}\right) + \mathbf{C}\left({}^{t}\dot{\mathbf{U}} + \frac{2}{\gamma\Delta t}{}^{t}\mathbf{U}\right) \tag{12}$$

Table 1
Attributes and parameters used in the Bathe time integration schemes (in all cases the Newmark parameters for the first sub-step are $\alpha = 0.25$, $\delta = 0.5$ to have the Trapezoidal rule).

Standard Bathe scheme [15,16,19,20]:
The parameter γ can be varied, but usually $\gamma = 0.5$; inherently $\rho_\infty = 0.0$

β_1/β_2**-Bathe scheme** [23]:
The parameter γ can in principle be varied but analysis was only given for $\gamma = 0.50$. The method is a 3-parameter method with β_1, β_2 and γ. More or less numerical dissipation can be achieved in a smooth manner; $\beta_2 = 1 - \beta_1$ is used for reduced numerical dissipation while maintaining second order accuracy; $\beta_2 = 2\beta_1$ is used for large numerical dissipation while providing first order accuracy

ρ_∞**-Bathe scheme**
The additional parameter to the standard Bathe scheme is ρ_∞. The method reduces to the standard Bathe scheme with $\rho_\infty = 0.0$; it reduces to the β_1/β_2-Bathe scheme with $s_0 = q_0 = \gamma(1-\beta_1)$, $s_1 = q_1 = \gamma(\beta_1+\beta_2-1)+1-\beta_2$ and $s_2 = q_2 = (1-\gamma)\beta_2$. The method is second-order accurate for any ρ_∞ and γ provided the relations in Eq. (14) are employed (but then no longer reduces to the β_1/β_2-Bathe scheme). Using $\gamma = \gamma_0$ given by ρ_∞ in Eq. (21), the scheme uses only one effective stiffness matrix and is a one-parameter method with optimal properties

$$\hat{\mathbf{R}}_2 = {}^{t+\Delta t}\mathbf{R} + \mathbf{M}\left(\frac{1}{\Delta t^2 q_2 s_2}{}^{t}\mathbf{U} + \frac{1}{\Delta t q_2 s_2}\left((q_0+q_2){}^{t}\dot{\mathbf{U}} + q_1{}^{t+\gamma\Delta t}\dot{\mathbf{U}}\right) + \frac{1}{s_2}\left(s_0{}^{t}\ddot{\mathbf{U}} + s_1{}^{t+\gamma\Delta t}\ddot{\mathbf{U}}\right)\right) + \mathbf{C}\left(\frac{1}{\Delta t q_2}{}^{t}\mathbf{U} + \frac{1}{q_2}\left(q_0{}^{t}\dot{\mathbf{U}} + q_1{}^{t+\gamma\Delta t}\dot{\mathbf{U}}\right)\right) \tag{13}$$

These relations are computationally quite similar to the relations using the standard Bathe method and the β_1/β_2-Bathe scheme.

2.1. Stability and accuracy characteristics of the ρ_∞-Bathe time integration method

To have second-order accuracy, we use, with and without physical damping included,

$$q_0 = (\gamma-1)q_1 + \frac{1}{2}$$
$$q_2 = -\gamma q_1 + \frac{1}{2} \tag{14}$$
$$s_0 = (\gamma-1)s_1 + \frac{1}{2}$$
$$s_2 = -\gamma s_1 + \frac{1}{2}$$

Note that with these conditions enforced the scheme no longer reduces to the β_1/β_2-Bathe method. In the decoupled modal equations, the method may be expressed as [1,24]

$$\begin{bmatrix} {}^{t+\Delta t}\ddot{x} \\ {}^{t+\Delta t}\dot{x} \\ {}^{t+\Delta t}x \end{bmatrix} = \mathbf{A}\begin{bmatrix} {}^{t}\ddot{x} \\ {}^{t}\dot{x} \\ {}^{t}x \end{bmatrix} + \mathbf{L_a}{}^{t+\gamma\Delta t}r + \mathbf{L_b}{}^{t+\Delta t}r \tag{15}$$

where $\mathbf{A}$, $\mathbf{L_a}$ and $\mathbf{L_b}$ are the integration approximation and load operators, respectively (see Appendix A). The stability and some accuracy characteristics of the method may be studied using this form of the scheme.

Using the relations in Eq. (14) and considering the case of no physical damping, the characteristic polynomial of $\mathbf{A}$ becomes

$$p(\lambda) = \lambda^3 - 2A_1\lambda^2 + A_2\lambda - A_3 \tag{16}$$

where

$$A_1 = \frac{1}{\beta_{01}\beta_{02}}(\gamma^2(q_1 s_1\gamma^2 - 2q_1 s_1\gamma + (q_1+s_1)(1/2) - 1/4)\Omega_0^4 + (-1 + (4q_1 s_1 + 1)\gamma^2 - 2(q_1+s_1)\gamma)\Omega_0^2 + 4));$$

$$A_2 = \frac{1}{\beta_{01}\beta_{02}}(\gamma^2(-2s_1 + \gamma s_1 + (1/2))(\gamma q_1 + (1/2) - 2q_1)\Omega_0^4 + (1 + (4q_1 s_1 + 1)\gamma^2 - 2(q_1+s_1)\gamma)\Omega_0^2 + 4)); \tag{17}$$

$$A_3 = 0;$$

$$\beta_{01} = \Omega_0^2\gamma^2 + 4; \quad \beta_{02} = 1 + (\gamma q_1 - (1/2))(\gamma s_1 - (1/2))\Omega_0^2$$

where ω_0 is the modal natural frequency and $\Omega_0 = \omega_0\Delta t$.

Using the Routh-Hurwitz stability criteria for Eq. (15), we obtain the useful relation for unconditional stability and the eigenvalues to be complex conjugate for all positive Ω_0:

$$s_1 = q_1 \tag{18}$$

Using Eq. (18) in Eq. (14) gives $s_0 = q_0$ and $s_2 = q_2$ and the coefficients in the approximations of the displacement and the velocity are identical, see Eqs. (6) and (7).

To directly prescribe the amount of numerical dissipation in the high frequency range, we use the relation between q_1 and the spectral radius in the high frequency range, ρ_∞:

$$q_1 = \frac{\rho_\infty + 1}{2\gamma(\rho_\infty - 1) + 4} \tag{19}$$

where

$$\rho_\infty = \lim_{\Omega_0\to\infty}\rho(\mathbf{A}), \quad \rho_\infty \in [0,1] \tag{20}$$

The scheme now has two free parameters, γ and ρ_∞. The step-by-step procedure of the method is summarized in Table 2. Note that, in practice, $\gamma = 0$, 1 and $2/(1-\rho_\infty)$ should be avoided since these values give zero denominators of constants in the method.

From Eqs. (10) and (11), we notice that the effective stiffness matrix in the first sub-step, $\hat{\mathbf{K}}_\mathbf{1}$, is identical to the one in the second sub-step, $\hat{\mathbf{K}}_\mathbf{2}$, when $s_2 = q_2 = \gamma/2$. Eqs. (14), (18) and (19) with $s_2 = q_2 = \gamma/2$ provide the expression of γ in terms of ρ_∞ to obtain identical effective stiffness matrices for all $\rho_\infty \in [0,1]$ as

$$\gamma_0 = \frac{2 - \sqrt{2+2\rho_\infty}}{1-\rho_\infty}; \quad \gamma_0 = 0.5 \text{ if } \rho_\infty = 1 \tag{21}$$

In Eq. (21), the value of γ_0 decreases from $2-\sqrt{2}$ to 0.5 as the value of ρ_∞ increases from 0 to 1. Note that for any value of $\rho_\infty \in [0,1]$, at γ_0 we have a local minimum of $\rho(\mathbf{A})$ (that is, $\rho(\mathbf{A})$ is smallest for a given $\Delta t/T$), a local maximum of the amplitude decay within the range of $\gamma \in (0,1)$, and the global minimum of the period elongation. In this sense we can refer to γ_0 as the optimal value of the method for any given ρ_∞ and using Eq. (21) the method is a one-parameter scheme.

Figs. 1–5 show the spectral radii, the amplitude decays and period elongations for various values of ρ_∞ and γ. Considering $\rho_\infty \in [0,1]$ and $\gamma \in (0,1)$ we have the largest amplitude decay and the smallest period elongation at γ_0 with the values decreasing and increasing, respectively, as γ is smaller and larger than γ_0. These results correspond to the observations given above. But for

Table 2
Step-by-step solution using the ρ_∞-Bathe method for linear analysis with general loading.

A. *Initial calculation*

1. Form stiffness matrix $\mathbf{K}$, lumped mass matrix $\mathbf{M}$, and damping matrix $\mathbf{C}$
2. Initialize ${}^0\mathbf{U}$, ${}^0\dot{\mathbf{U}}$ and ${}^0\ddot{\mathbf{U}}$.
3. Select time step Δt, ρ_∞ (default = 0.0), γ (default = γ_0 in Eq. (21)), and calculate integration constants:

$$q_1 = \frac{\rho_\infty+1}{2\gamma(\rho_\infty-1)+4};\quad q_0 = (\gamma-1)q_1+\tfrac{1}{2};\quad q_2 = -\gamma q_1+\tfrac{1}{2}$$
$$a_0 = \frac{4}{\gamma^2\Delta t^2};\quad a_1 = \frac{2}{\gamma\Delta t};\quad a_2 = \frac{1}{\Delta t^2 q_2^2};\quad a_3 = \frac{1}{\Delta t q_2};\quad a_4 = \frac{4}{\gamma\Delta t};$$
$$a_5 = \frac{q_0+q_2}{\Delta t q_2^2};\quad a_6 = \frac{q_1}{\Delta t q_2^2};\quad a_7 = \frac{q_0}{q_2};\quad a_8 = \frac{q_1}{q_2};$$

4. Form effective stiffness matrix $\hat{\mathbf{K}}_1$ and $\hat{\mathbf{K}}_2$:
$\hat{\mathbf{K}}_1 = \mathbf{K}+a_0\mathbf{M}+a_1\mathbf{C};\quad \hat{\mathbf{K}}_2 = \mathbf{K}+a_2\mathbf{M}+a_3\mathbf{C};$
5. Triangularize $\hat{\mathbf{K}}_1$ and $\hat{\mathbf{K}}_2$: $\hat{\mathbf{K}}_1 = \mathbf{L}_1\mathbf{D}_1\mathbf{L}_1^{\mathrm{T}};\quad \hat{\mathbf{K}}_2 = \mathbf{L}_2\mathbf{D}_2\mathbf{L}_2^{\mathrm{T}}$

B. *For each time step:*

<First sub-step>

1. Calculate effective loads at time $t+\gamma\Delta t$:
$${}^{t+\gamma\Delta t}\hat{\mathbf{R}} = {}^{t+\gamma\Delta t}\mathbf{R}+\mathbf{M}\left({}^{t}\ddot{\mathbf{U}}+a_4{}^{t}\dot{\mathbf{U}}+a_0{}^{t}\mathbf{U}\right)+\mathbf{C}\left({}^{t}\dot{\mathbf{U}}+a_1{}^{t}\mathbf{U}\right)$$
2. Solve for displacements at time $t+\gamma\Delta t$:
$$\mathbf{L}_1\mathbf{D}_1\mathbf{L}_1^{\mathrm{T}}{}^{t+\gamma\Delta t}\mathbf{U} = {}^{t+\gamma\Delta t}\hat{\mathbf{R}}$$
3. Calculate velocities and accelrations at time $t+\gamma\Delta t$:
$${}^{t+\gamma\Delta t}\dot{\mathbf{U}} = a_1\left({}^{t+\gamma\Delta t}\mathbf{U}-{}^{t}\mathbf{U}\right)-{}^{t}\dot{\mathbf{U}}$$
$${}^{t+\gamma\Delta t}\ddot{\mathbf{U}} = a_1\left({}^{t+\gamma\Delta t}\dot{\mathbf{U}}-{}^{t}\dot{\mathbf{U}}\right)-{}^{t}\ddot{\mathbf{U}}$$

<Second sub-step>

1. Calculate effective loads at time $t+\Delta t$:
$${}^{t+\Delta t}\hat{\mathbf{R}} = {}^{t+\Delta t}\mathbf{R}+\mathbf{M}\left(a_2{}^{t}\mathbf{U}+a_5{}^{t}\dot{\mathbf{U}}+a_6{}^{t+\gamma\Delta t}\dot{\mathbf{U}}+a_7{}^{t}\ddot{\mathbf{U}}+a_8{}^{t+\gamma\Delta t}\ddot{\mathbf{U}}\right)$$
$$+\mathbf{C}\left(a_3{}^{t}\mathbf{U}+a_7{}^{t}\dot{\mathbf{U}}+a_8{}^{t+\gamma\Delta t}\dot{\mathbf{U}}\right)$$
2. Solve for displacements at time $t+\Delta t$:
$$\mathbf{L}_2\mathbf{D}_2\mathbf{L}_2^{\mathrm{T}}{}^{t+\Delta t}\mathbf{U} = {}^{t+\Delta t}\hat{\mathbf{R}}$$
3. Calculate velocities and accelrations at time $t+\Delta t$:
$${}^{t+\Delta t}\dot{\mathbf{U}} = -a_3{}^{t}\mathbf{U}+a_3{}^{t+\Delta t}\mathbf{U}-a_7{}^{t}\dot{\mathbf{U}}-a_8{}^{t+\gamma\Delta t}\dot{\mathbf{U}}$$
$${}^{t+\Delta t}\ddot{\mathbf{U}} = -a_3{}^{t}\dot{\mathbf{U}}+a_3{}^{t+\Delta t}\dot{\mathbf{U}}-a_7{}^{t}\ddot{\mathbf{U}}-a_8{}^{t+\gamma\Delta t}\ddot{\mathbf{U}}$$

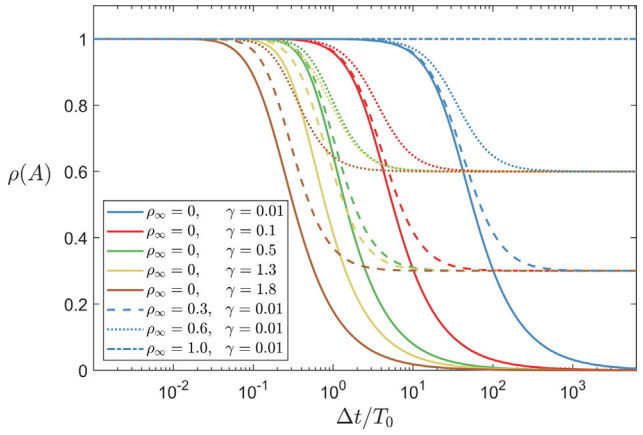

Fig. 1. Spectral radii of approximation operator of the ρ_∞-Bathe method when $\xi = 0$ for various values of γ and ρ_∞; Each color indicates a value of γ; Each line type indicates a value of ρ_∞: solid ($\rho_\infty = 0$), dashed ($\rho_\infty = 0.3$), dotted ($\rho_\infty = 0.6$), dashed dot ($\rho_\infty = 1$); The curves with solid line ($\rho_\infty = 0$) are identical to the curves of the standard Bathe method with the same γ. (For interpretation of the references to color in this figure legend, the reader is referred to the web version of this article.)

$\gamma \in (1, 2/(1-\rho_\infty))$, both the amplitude decay and period elongation increase as γ increases. Also, as γ approaches 0 or 1, for all $\rho_\infty \in [0,1]$, the properties of the method approach those of the single-step trapezoidal rule. Finally, we note that for all $\rho_\infty \in [0,1]$, the properties of the method change with γ in the same way as the properties change in the standard Bathe method, see in particular Fig. 1.

Considering γ_0, as ρ_∞ increases from 0 to 1, both, the amplitude decay and the period elongation are reduced. However, with $\gamma \in (1, 2/(1-\rho_\infty))$, as ρ_∞ increases, the amplitude decay decreases significantly while the change in the period elongation is small.

It is interesting to note that the relation between the splitting ratio γ and spectral radius ρ_∞ shown in Eq. (21) is identical to the relation between the splitting ratio p and the spectral radius at the bifurcation point ρ_b in an explicit time integration method proposed by the authors [3].

As in the standard Bathe method, the spectral properties of the ρ_∞-Bathe scheme for a given ρ_∞ possess symmetry (with some scaling) with respect to γ, where the center of the symmetry is γ_0: namely γ and $2(1-\gamma)/(2-\gamma+\gamma\rho_\infty)$ provide an identical characteristic polynomial in Eq. (16), hence the same spectral properties arise. With $\rho_\infty = 0$, the symmetry in the spectral properties of the ρ_∞-Bathe scheme is identical to that of the standard Bathe method [20].

Due to the symmetry with respect to γ, with $\rho_\infty \in [0,1]$, the spectral properties of $\gamma \in (0, \gamma_0)$ can be reproduced by using $\gamma \in (\gamma_0, 1)$, where $\gamma \in (1, 2/(1-\rho_\infty))$ has its counterpart in $\gamma \in (-\infty, 0)$. For example, with $\rho_\infty = 0.5$, the curves of the spectral radius, the amplitude decay and the period elongation for $\gamma = 0.3$ are identical to those for $\gamma = 0.757$ (the value is rounded). We refer to Ref. [20] for comments on the use of negative values of γ.

2.2. Similarities and differences to the standard Bathe and β_1/β_2-Bathe methods

Considering $\rho_\infty = 0$, the method is spectrally identical to the standard Bathe method: an identical characteristic polynomial in Eq. (16) is obtained. Moreover, for nonzero ρ_∞ values, the method shows various desired characteristics of the standard Bathe method, but of course with the effects of nonzero ρ_∞. For $\rho_\infty = 1$, the method has no amplitude decay for all frequencies, and with $\gamma = 0.5$ which is γ_0 for $\rho_\infty = 1$, the method provides the performance of the two-step trapezoidal rule.

In the standard Bathe method, the splitting ratio $\gamma = 2-\sqrt{2}$ provides identical effective stiffness matrices for the two sub-steps, the local minimum of $\rho(\mathbf{A})$, the local maximum of amplitude decay and the global minimum of the period elongation: this splitting ratio is obtained in Eq. (21) with $\rho_\infty = 0$. Also, with $\rho_\infty = 0$, the symmetry in the spectral properties of the standard Bathe method is recovered. Furthermore we note that for all $\rho_\infty \in [0,1]$, the amplitude decays and period elongations of the ρ_∞-Bathe scheme change with γ in the same way as when $\rho_\infty = 0$, that is, in the standard Bathe method. Hence we can interpret the scheme as a "Bathe method with controllable ρ_∞."

Recently, the β_1/β_2-Bathe scheme was proposed to change the amplitude decay in the standard Bathe method [23]. The values $\beta_2 = 2\beta_1$ (for $\beta_1 \in [1/3, \infty)$) and $\beta_2 = 1-\beta_1$ (for $\beta_1 \in [1/3, 1/2]$) are used (with $\gamma = 1/2$) to have more or less numerical dissipation than obtained in the standard Bathe method.

In the β_1/β_2-Bathe scheme, second order accuracy can only be obtained by satisfying

$$(\beta_1+\beta_2-1)\gamma^2+(1-2\beta_2)\gamma+\beta_2-\frac{1}{2} = 0 \tag{22}$$

Therefore, for $\gamma = 1/2$, only $\beta_2 = 1-\beta_1$ provides second order accuracy. The only case of second-order accuracy with $\beta_2 = 2\beta_1$ (with the condition $\beta_2 = 1-\beta_1$) is $\beta_1 = 1/3$ and $\beta_2 = 2/3$, which is when the β_1/β_2-Bathe method reduces to the standard Bathe method. Therefore, while the amplitude decay can be smoothly increased to provide a larger numerical dissipation than obtained in the standard Bathe method with $\gamma = 1/2$, the β_1/β_2-Bathe scheme is then only a first-order accurate method. Note that the ρ_∞-Bathe method

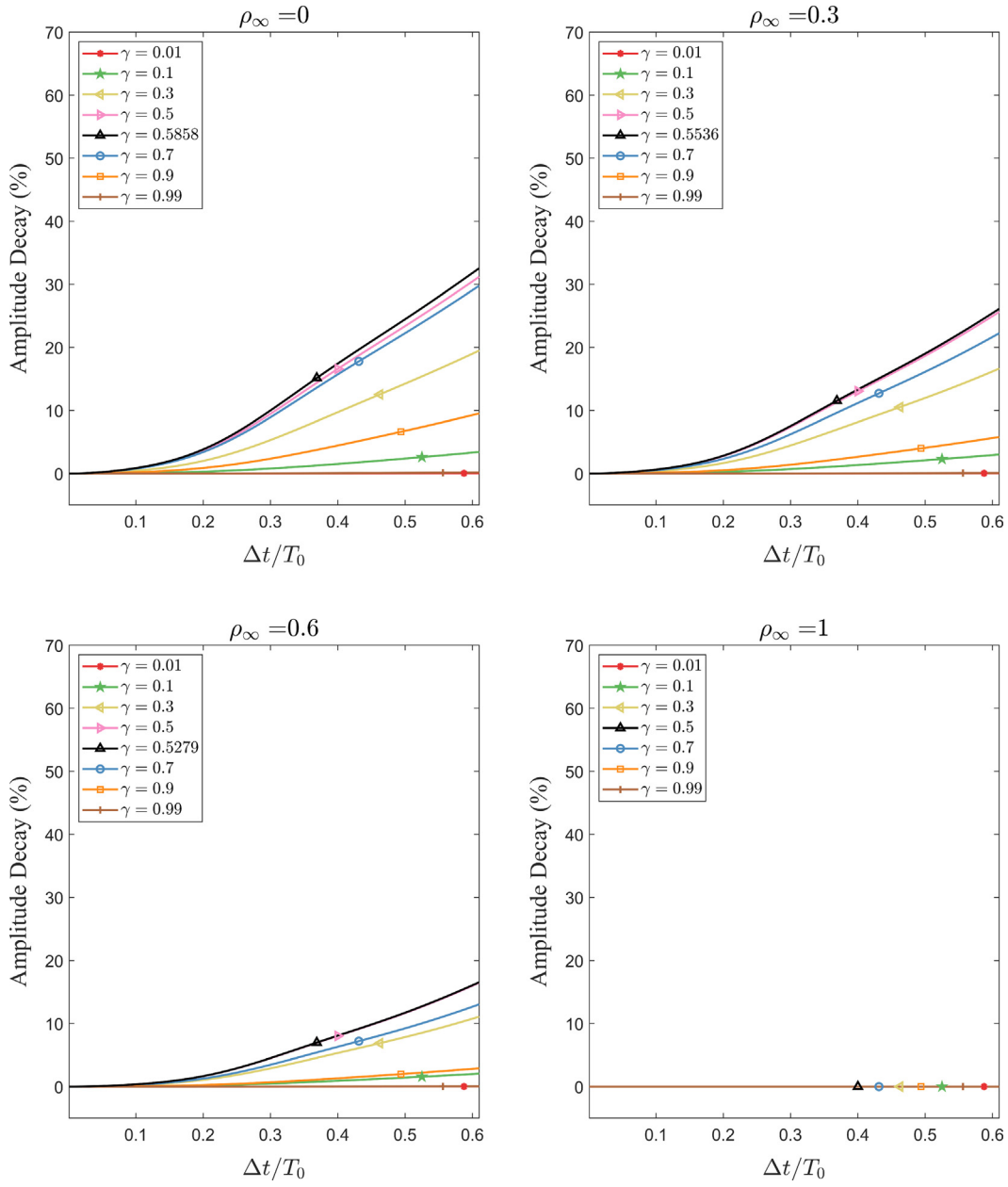

Fig. 2. Percentage amplitude decays of the ρ_∞-Bathe method when $\xi = 0$ for various values of $\gamma \in (0, 1)$ and ρ_∞.

always provides second-order accuracy for all possible values of γ and ρ_∞ since the conditions in Eq. (14) are imposed.

A major advantage of the β_1/β_2-Bathe method over the standard Bathe method is that for the least numerical dissipation and dispersion, the method can be used as the two-step trapezoidal rule while the standard Bathe method can only provide the performance of the one-step trapezoidal rule but using the two substeps. Note that the ρ_∞-Bathe method also provides the performance of the two-step trapezoidal rule with $\rho_\infty = 1$ and $\gamma = 0.5$.

With specific values of β_1 and β_2, the β_1/β_2-Bathe scheme reduces to the standard Bathe method and using a specific value γ also the two coefficient matrices are identical. However, three parameters are in essence used. Therefore, while using the β_1, β_2 parameters and possibly γ the amount of numerical dissipation and dispersion can be smoothly changed to have small or large values, the use of γ and ρ_∞ in the ρ_∞-Bathe scheme is simpler because less parameters are used and the scheme for any $\rho_\infty \in [0, 1]$ behaves as the standard Bathe method, as an analyst may like to have in practical solutions.

Regarding the usage of the ρ_∞-Bathe method, we recommend to use $\rho_\infty = 0$, the standard Bathe method, with $\gamma = 0.5$ or $2 - \sqrt{2}$, as the default setting for general structural dynamics problems, see Section 3.1. If we understand the characteristics of the dynamic problem to be solved a priori or after studying the numerical results obtained using the default values, we may use other values of γ and ρ_∞ for enhanced accuracy. For problems which do not require high numerical damping in the high frequency range, we may use $\rho_\infty \in [0, 1]$ with $\gamma = \gamma_0$ in Eq. (21) for reduced amplitude decays and period elongations; namely, as ρ_∞ approaches 1 from 0, the method gives less amplitude decay and period elongation. The usefulness of nonzero ρ_∞ values is illustrated in Section 3.2. For the solution of a problem requiring large numerical dissipation, like problems of wave propagations, we may use $\rho_\infty = 0$ with $\gamma > 1.3$, see. Section 3.3.

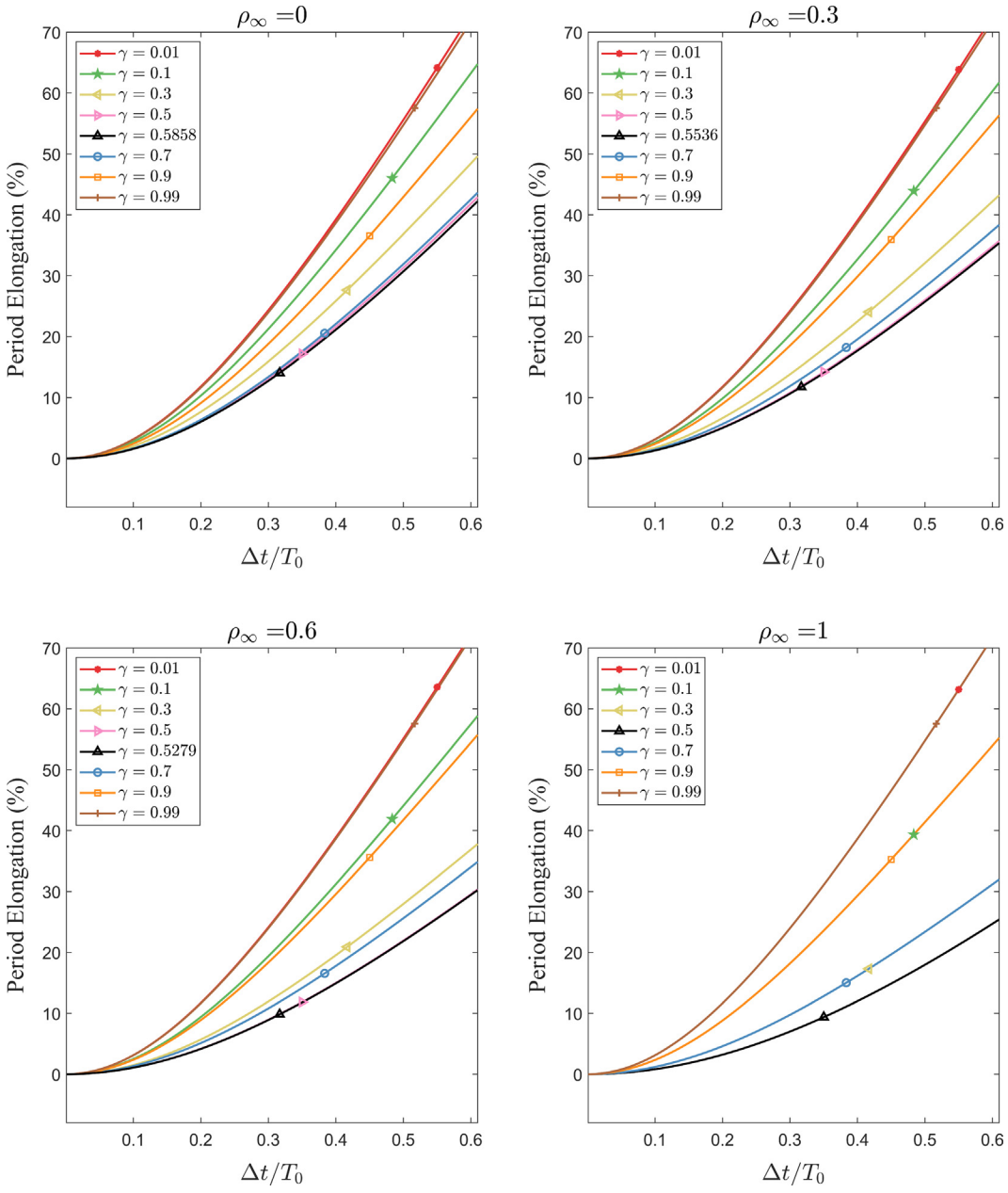

Fig. 3. Percentage period elongations of the ρ_∞-Bathe method when $\xi = 0$ for various values of $\gamma \in (0, 1)$ and ρ_∞.

3. Illustrative solutions

We consider a 3 degree-of-freedom model problem and a 1D wave propagation problem to illustrate the behavior of the ρ_∞-Bathe method. For the model problem, we consider two cases: $k_1 = 10^7$ and 5.

3.1. Three degree-of-freedom spring system: stiff-soft spring case

We first consider the case of $k_1 = 10^7$ in the model problem shown in Fig. 6. This problem was already used in Refs. [19,20] to represent a general structure with stiff and flexible parts. We refer to Refs. [19,1] for comments on the importance of the problem.

Figs. 7–15 show the results obtained using various time integration methods – the $\text{U0V0}_{\text{optimal}}$ scheme presented by Zhou and Tamma as a U0-V0 scheme [11], the three-parameter method (or generalized-α method) [12–14], the standard Bathe method, a one-parameter composite method using ρ_∞ proposed by Kim and Choi [22], and the ρ_∞-Bathe method. In all solutions, we use $\Delta t = 0.5236$ with the period of the external loading $T_p \simeq 5.236$. For the standard Bathe method, we use $\alpha = 1/4$, $\delta = 1/2$ with $\gamma = 0.5$ and 0.9. We use the parameter values $\rho_\infty = 0$ and 0.3 for the $\text{U0V0}_{\text{optimal}}$, three-parameter and one-parameter methods. For the ρ_∞-Bathe method, we consider $\gamma = 0.5$ with $\rho_\infty = 0$ and 0.3.

The standard Bathe method with $\gamma = 0.5$ and the ρ_∞-Bathe method with $\gamma = 0.5$ and $\rho_\infty = 0$ provide identical results (as expected, see Section 2) and the best results, indeed with other γ values for the standard Bathe scheme and other values of ρ_∞ for the ρ_∞-Bathe method, the accuracy is decreased. The results using the other methods are not satisfactory. For the 3-parameter method and the one-parameter composite method, a smaller ρ_∞ value provides better accuracy and, interestingly, the $\text{U0V0}_{\text{optimal}}$ scheme provides the same results for the values ρ_∞ considered.

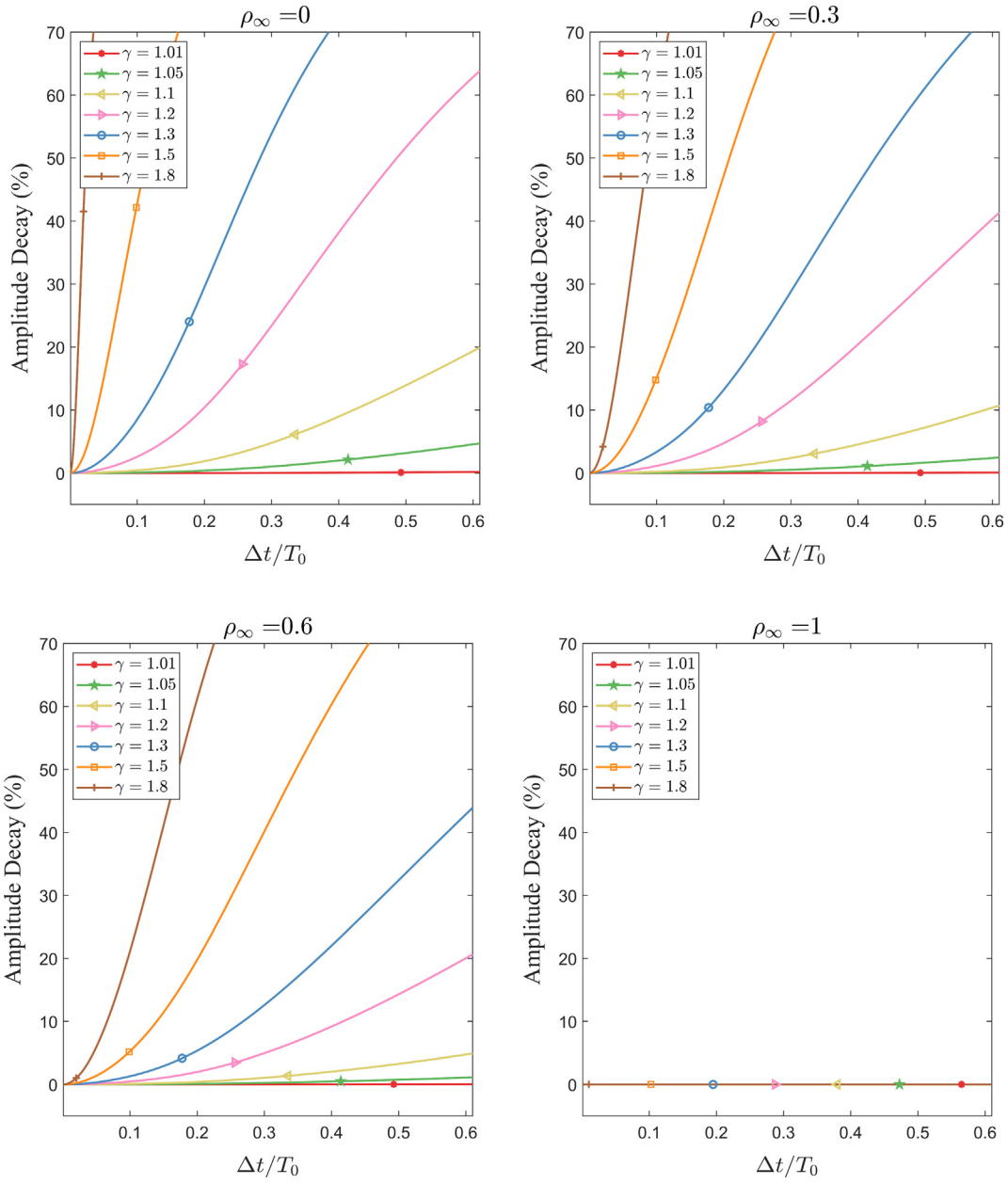

Fig. 4. Percentage amplitude decays of the ρ_∞-Bathe method when $\xi = 0$ for various values of $\gamma > 1$ and ρ_∞.

This example solution shows the importance of the rapid suppression of spurious response in the higher mode. Also, for the acceleration at node 2 and the reaction, the ρ_∞-Bathe scheme and the one-parameter composite method provide practically the same results for the first step (see. Figs. 12 and 15), while only the ρ_∞-Bathe method provides satisfactory results for the rest of the time steps.

Note that in the standard Bathe method, and equivalently in the ρ_∞-Bathe method with $\rho_\infty = 0$, there is a first time step overshoot in the acceleration at node 2 and in the reaction. This error can be eliminated by using a different set of α and δ only for the first substep, see Refs. [1,20] for the details.

3.2. Three degree-of-freedom spring system: soft-soft spring case

We now consider the 3-degree-of-freedom model problem of Fig. 6 with $k_1 = 5$ as a problem with no spurious high frequency. We use $\Delta t = 0.25$ for the standard Bathe, the one-parameter composite, and the ρ_∞-Bathe methods.

In this case all frequencies should be integrated quite accurately. Hence we use $\rho_\infty = 0.99$ for the one-parameter composite method and the ρ_∞-Bathe scheme with $\gamma = 0.5$. With both methods, as ρ_∞ increases from 0 to 1, the amplitude decays and the period elongations are minimized. For the standard Bathe method, we consider $\gamma = 0.5$ and 0.9.

Figs. 16 and 17 show the calculated reactions. As expected, using the ρ_∞-Bathe and the one-parameter composite methods with $\rho_\infty = 0.99$ gives accurate and practically the same results. Using the standard Bathe method with $\gamma = 0.5$ provides better results than when using $\gamma = 0.9$.

These results indicate the usefulness of using $\rho_\infty \neq 0$ in the ρ_∞-Bathe method for the solution of problems when no spurious high frequencies are to be eliminated. However, in practice, the judicious use of ρ_∞ other than zero may require some numerical experimentation.

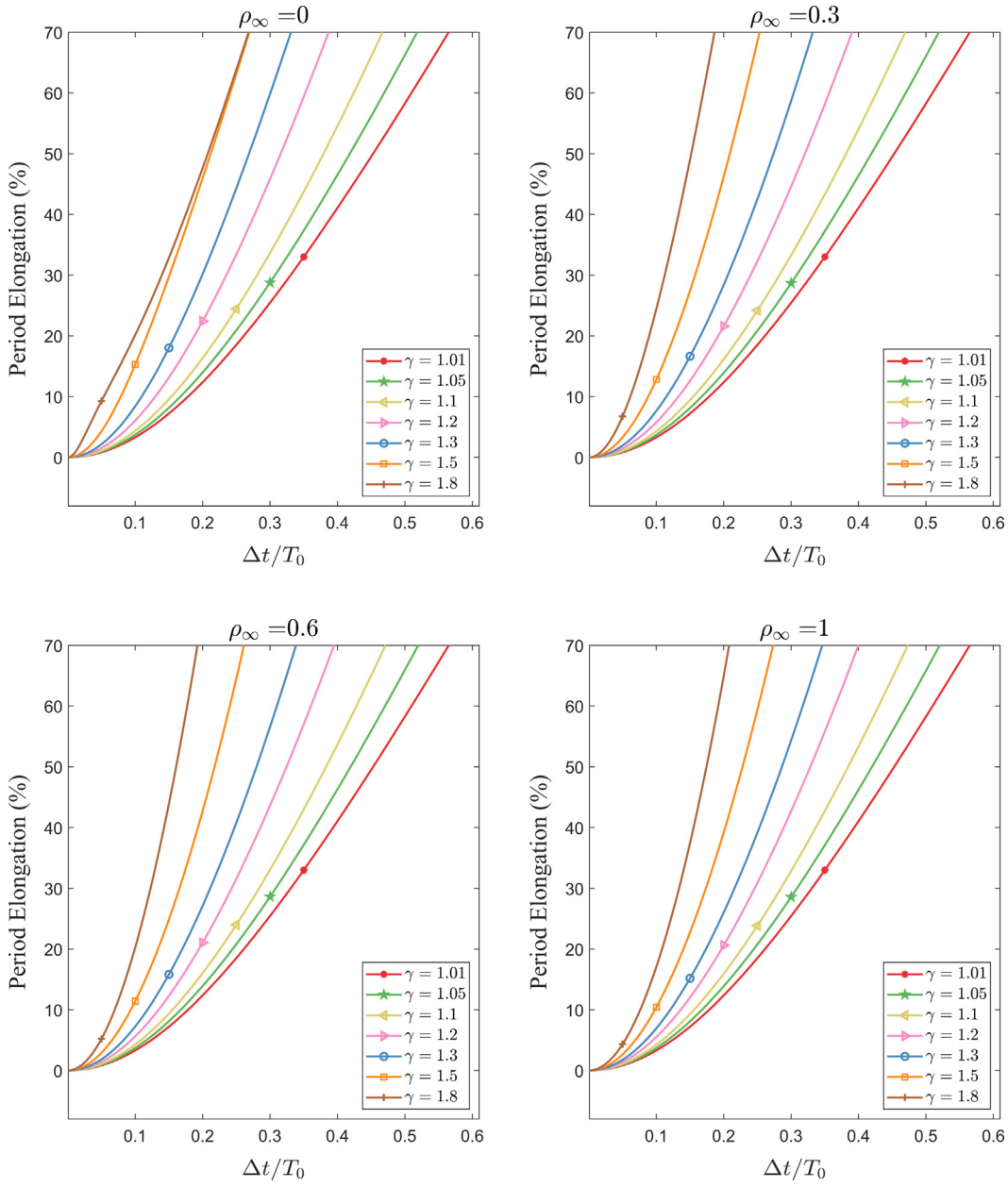

Fig. 5. Percentage period elongations of the ρ_∞-Bathe method when $\xi = 0$ for various values of $\gamma > 1$ and ρ_∞.

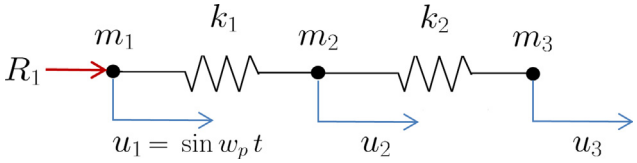

Fig. 6. Model problem of three degrees of freedom spring system, $k_2 = 1$, $m_1 = 0$, $m_2 = 1$, $m_3 = 1$, $\omega_p = 1.2$, $k_1 = 10^7$ or 5.

3.3. One-dimensional wave propagation in a clamped-free bar

In this solution we consider the 1D wave propagation problem shown in Fig. 18 [25,23]. A clamped bar is excited by a constant external load at its end, $F(t) = 10^4$, and the material and geometrical constants are Young's modulus $E = 3 \times 10^7$, mass density $\rho = 0.00073$, cross-sectional area $A = 1$, and length $L = 200$. We use 1000 equal size two-node elements. This problem was also solved using these data in Ref. [23].

In wave propagation analysis using an implicit time integration, high numerical dissipation is frequently desired to suppress spurious modes [21,26]. Therefore, we use the ρ_∞-Bathe method with $\gamma = 1.99$ and $\rho_\infty = 0$, the standard Bathe method with $\gamma = 1.99$, and the one-parameter composite method with $\rho_\infty = 0$. For the time step size, we use two CFL numbers, 0.1 and 1. The CFL number is the ratio of the propagation length per time step (using the exact wave speed) to the element size: $\Delta t_1 = 9.8658 \times 10^{-8}$ and $\Delta t_2 = 9.8658 \times 10^{-7}$. The computed results are given in Figs. 19 and 20.

All methods with the considered parameters predict the displacement at the center of the bar (at node 500) accurately (Fig. 19), while for the velocity at the same point, there are spurious oscillations in the results using the one-parameter composite

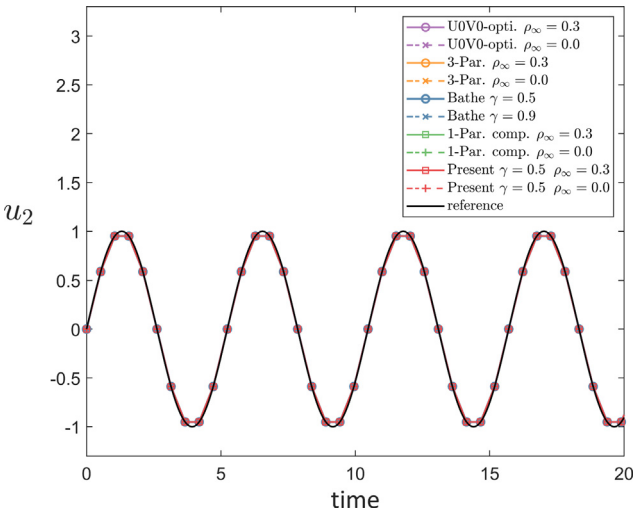

Fig. 7. Displacement of node 2 for various methods; The U0V0 method is described in Ref. [11], the 3-Par. method is described in Refs. [12–14] and the 1-Par. comp. method is described in Ref. [22].

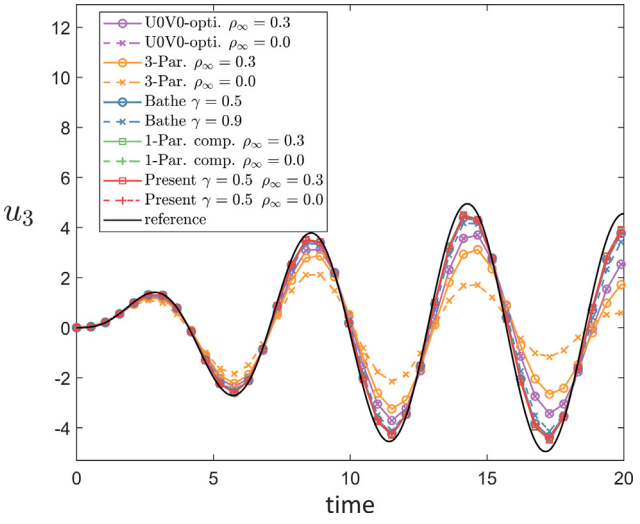

Fig. 8. Displacement of node 3 for various methods for $k_1 = 10^7$.

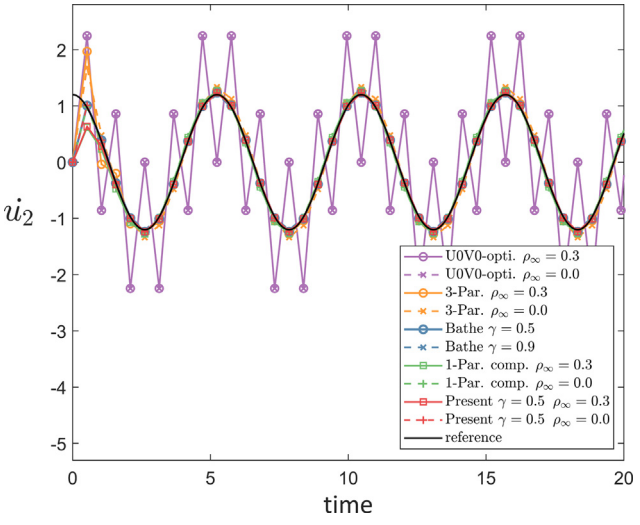

Fig. 9. Velocity of node 2 for various methods for $k_1 = 10^7$ (the static correction gives the nonzero velocity at time = 0.0).

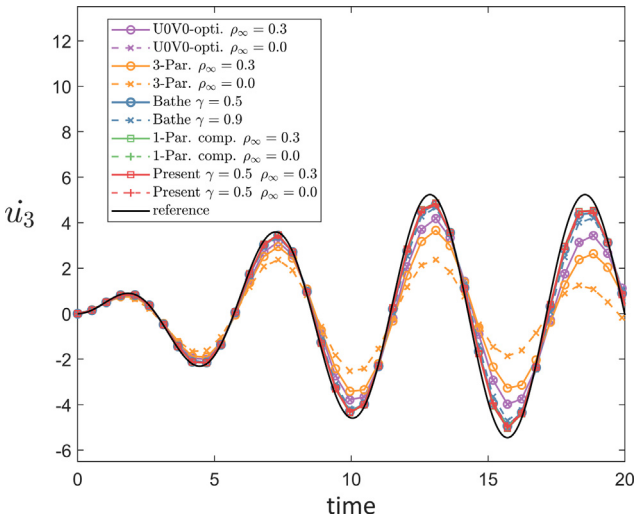

Fig. 10. Velocity of node 3 for various methods for $k_1 = 10^7$.

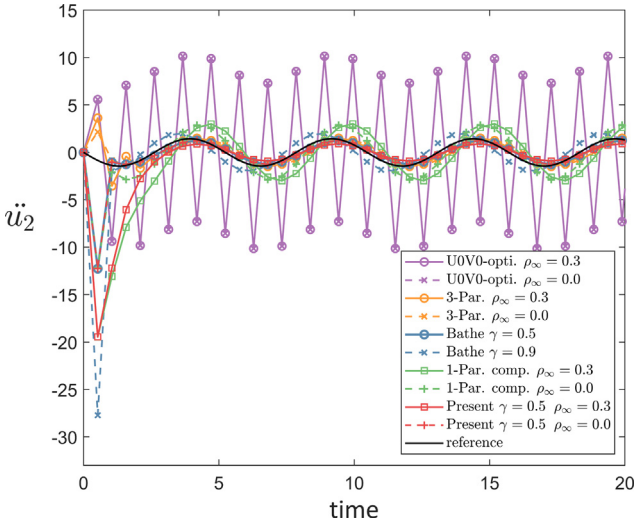

Fig. 11. Acceleration of node 2 for various methods for $k_1 = 10^7$.

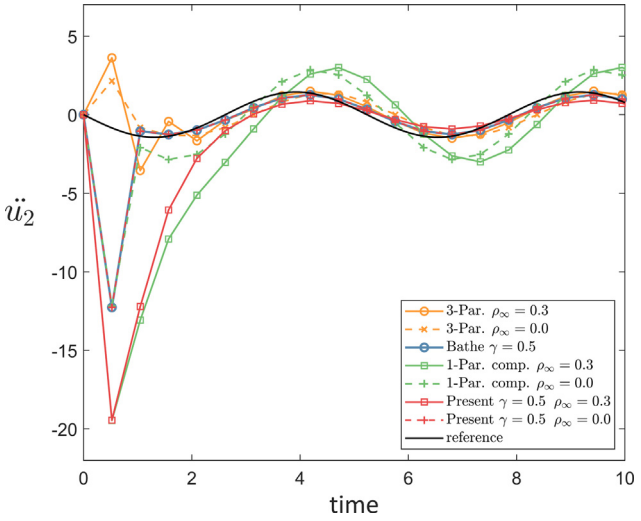

Fig. 12. Close-up of acceleration of node 2 for various methods for $k_1 = 10^7$.

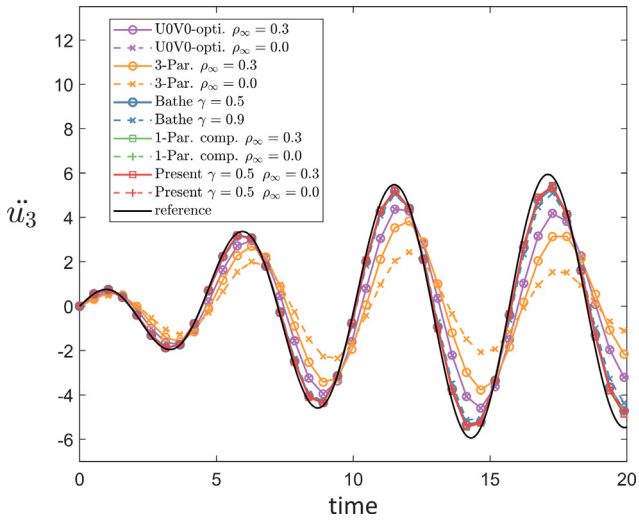

Fig. 13. Acceleration of node 3 for various methods for $k_1 = 10^7$.

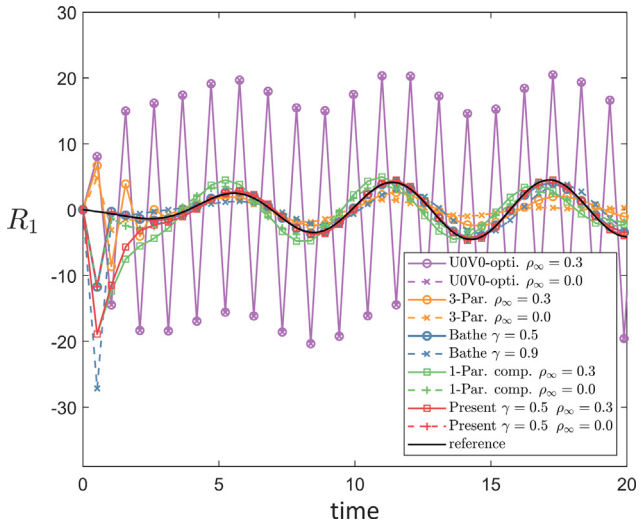

Fig. 14. Reaction force at node 1 for various methods for $k_1 = 10^7$.

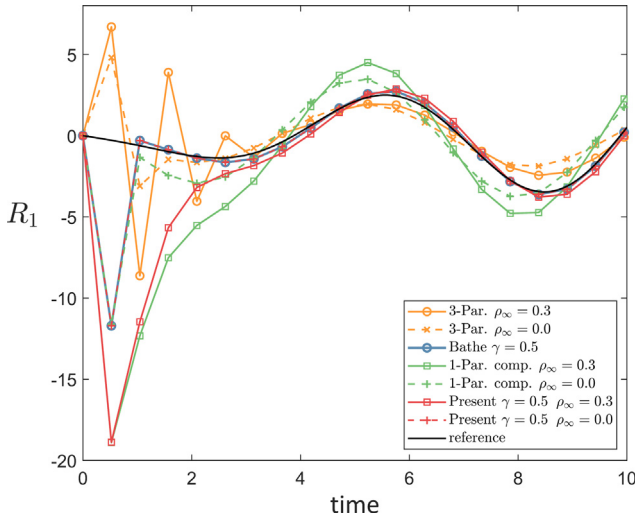

Fig. 15. Close-up of reaction force at node 1 for various methods for $k_1 = 10^7$.

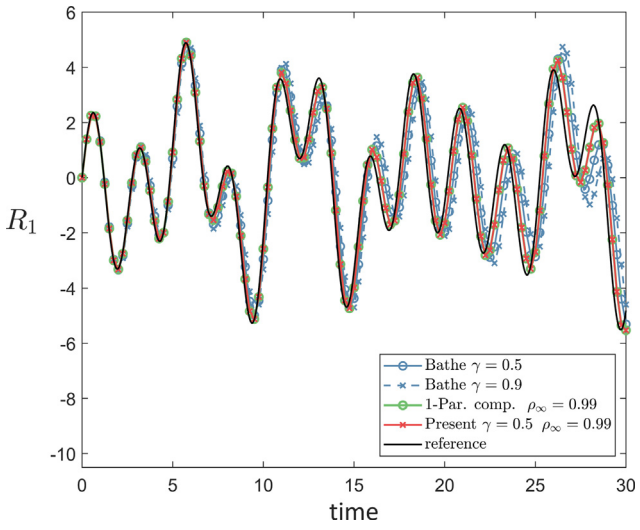

Fig. 16. Reaction force at node 1 for various methods for $k_1 = 5$.

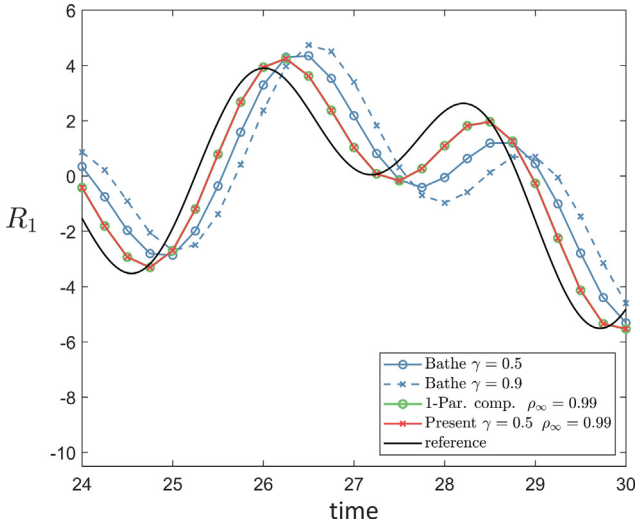

Fig. 17. Close-up of reaction force at node 1 for various methods for $k_1 = 5$.

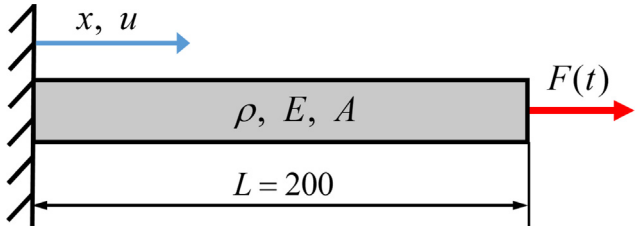

Fig. 18. A clamped-free bar excited by end load.

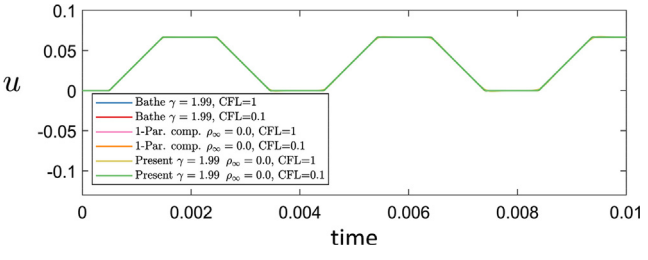

Fig. 19. Displacement at $x = 100$ for various methods.

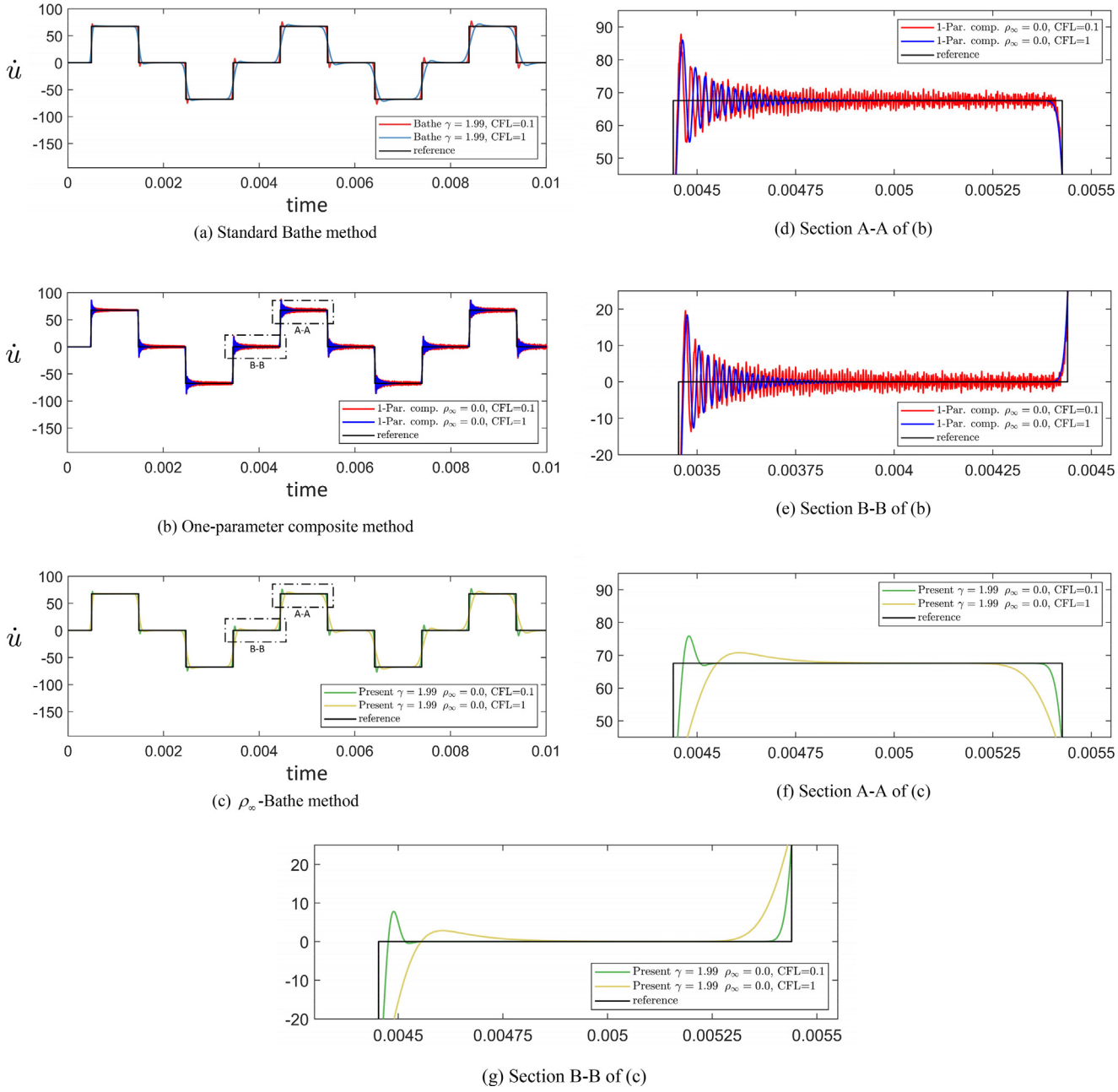

(a) Standard Bathe method

(b) One-parameter composite method

(c) ρ_∞-Bathe method

(d) Section A-A of (b)

(e) Section B-B of (b)

(f) Section A-A of (c)

(g) Section B-B of (c)

Fig. 20. Velocity at $x = 100$ for various methods.

method for both CFL numbers considered. Since in the one-parameter composite method the smallest value of ρ_∞ is used already, a further suppression of spurious oscillations cannot be expected for the time step sizes used. The standard Bathe method and the ρ_∞-Bathe method with $\rho_\infty = 0$ provide the same results, as expected, and perform reasonably well using both CFL numbers. We see that using CFL = 0.1 in the Bathe scheme provides a solution showing more accurately the step change in velocity but with a larger overshoot. However, a further study is needed to identify the CFL number for optimal accuracy of the methods with various values of γ [26]. We note that the β_1/β_2-Bathe method provides remarkably accurate solutions for this problem with $\beta_2 = 2\beta_1$ although only being a first-order accurate method. We refer to Ref. [23] for the solutions using the β_1/β_2-Bathe method. Hence the first order method may give quite accurate results for this type of problem, but this observation requires more research.

4. Concluding remarks

We considered the standard Bathe time integration scheme with the objective to be able to prescribe ranges of numerical dissipation and dispersion for the numerical integration of finite element equations. To achieve this aim, we proposed to use the trapezoidal rule for the first sub-step and a set of relations between the solution variables for the second sub-step. In its final form, the method has two parameters: the time step splitting ratio, γ, and the spectral radius at large time step sizes, ρ_∞. We refer to the method as the ρ_∞-Bathe scheme.

With $\rho_\infty = 0$, the method reduces to the standard Bathe method for any value of γ. For values of ρ_∞ other than zero, the ρ_∞-Bathe method shows the same change in accuracy characteristics for any γ value as when using $\rho_\infty = 0$. When $\rho_\infty = 1$ and $\gamma = 1/2$, the method is the two-step trapezoidal rule.

Hence for the solution of problems for which the errors in predicted amplitudes and periods should be small, a value $\rho_\infty \neq 0$ can be used with the γ value determined by ρ_∞ for optimal accuracy. Then the method is a one-parameter method.

In general, values of ρ_∞ and γ can be used to adjust the solution accuracy of the method in a smooth manner, namely from including no dissipation to very large dissipation, with correspondingly small period elongation to very large period elongation, while maintaining second-order accuracy.

In this paper, we focused on the development and basic properties of the ρ_∞-Bathe method. Further studies on its performance and the optimal usage in the analysis of wave propagations would be very valuable, in particular when used with overlapping finite elements [27].

Acknowledgement

This work was partly supported by the Basic Science Research Program (Grant No. 2018R1D1A1B07045805) through the National Research Foundation of Korea (NRF) funded by the Ministry of Education.

Appendix A. The integration operator $\mathbf{A}$ and the load operators $\mathbf{L}_a$ and $\mathbf{L}_b$

$$\mathbf{A} = \frac{1}{\kappa_1\kappa_2}\begin{bmatrix} a_{11} & a_{12} & a_{13} \\ a_{21} & a_{22} & a_{23} \\ a_{31} & a_{32} & a_{33} \end{bmatrix}$$

$$\mathbf{L_a} = \frac{1}{\kappa_1\kappa_2}\begin{bmatrix} -2\Omega_0((\gamma q_1 + 2s_1q_2)\Omega_0 + 4\xi s_1) \\ -2\Delta t\left(\Omega_0^2 q_1\gamma s_2 - 2s_1\right) \\ 4\Delta t^2(\Omega_0 q_1\gamma s_2\xi + (1/2)\gamma q_1 + s_1q_2) \end{bmatrix}$$

$$\mathbf{L_b} = \frac{1}{\kappa_1\kappa_2}\begin{bmatrix} \Omega_0^2\gamma^2 + 4\Omega_0\gamma\xi + 4 \\ s_2\Delta t\left(\Omega_0^2\gamma^2 + 4\Omega_0\gamma\xi + 4\right) \\ q_2s_2\Delta t^2\left(\Omega_0^2\gamma^2 + 4\Omega_0\gamma\xi + 4\right) \end{bmatrix}$$

where

$$\kappa_1 = \Omega_0^2\gamma^2 + 4\Omega_0\gamma\xi + 4$$

$$\kappa_2 = \Omega_0^2 q_2 s_2 + 2\Omega_0 s_2\xi + 1$$

$$a_{11} = -2\Omega_0\begin{pmatrix} (1/2)\gamma^2 q_2(s_0 - s_1)\Omega_0^3 + 2\gamma\xi(\gamma/2 + q_2)(s_0 - s_1)\Omega_0^2 \\ +\left((4(s_0 - s_1)\xi^2 + q_1)\gamma + 2q_2s_0\right)\Omega_0 + 4s_0\xi \end{pmatrix}$$

$$a_{12} = \frac{-4\Omega_0}{\Delta t}\begin{pmatrix} (1/4)((q_0 - q_1 + q_2)\gamma - 4s_1q_2)\gamma\Omega_0^3 + \left((1/2)\gamma^2\right. \\ +(q_0 + q_2 - 2s_1)\gamma - 2s_1q_2)\xi\Omega_0^2 \\ \left.+(2\gamma\xi^2 - 4s_1\xi^2 + q_0 + q_1 + q_2)\Omega_0 + 2\xi\right. \end{pmatrix}$$

$$a_{13} = \frac{2\Omega_0^2}{\Delta t^2}\left(-2 + \left(\gamma q_1 + 2s_1q_2 - (1/2)\gamma^2\right)\Omega_0^2 + 4(s_1 - (\gamma/2))\xi\Omega_0\right)$$

$$a_{21} = -2\Delta t\left(\gamma((-s_0 + s_1)(\gamma/2) + s_2q_1)\Omega_0^2 - 2\gamma\xi\Omega_0(s_0 - s_1) - 2s_0\right)$$

$$a_{22} = 4 - \gamma^2 s_2\Omega_0^4(q_0 - q_1) - 4\Omega_0^3\gamma s_2\xi q_0 + \left(\gamma^2 - 4s_1\gamma - 4s_2(q_0 + q_1)\right)\Omega_0^2 - 8(s_1 - (\gamma/2))\xi\Omega_0$$

$$a_{23} = \frac{2\Omega_0^2}{\Delta t}\left(s_2\gamma(q_1 - (\gamma/2))\Omega_0^2 - 2\gamma s_2\xi\Omega_0 - 2s_1 - 2s_2\right)$$

$$a_{31} = 4\Delta t^2\left((1/4)\gamma^2 q_2\Omega_0^2(s_0 - s_1) + (((s_0 - s_1)q_2 + s_2q_1)\xi\Omega_0 + (q_1/2))\gamma + q_2s_0\right)$$

$$a_{32} = 8\Delta t\begin{pmatrix} (1/4)s_2\xi(q_0 - q_1)\Omega_0^3\gamma^2 \\ +\left((q_0 - q_1 + q_2)(\gamma/8) + s_2\xi^2 q_0 - (1/2)s_1q_2\right)\gamma\Omega_0^2 \\ +((q_0 + q_2)(\gamma/2) + s_2q_0 + s_2q_1 - s_1q_2)\xi\Omega_0 + (1/2)(q_0 + q_1 + q_2) \end{pmatrix}$$

$$a_{33} = 4 - 4(q_1 - (\gamma/2))s_2\gamma\xi\Omega_0^3 + \left(\gamma^2 + \left(8s_2\xi^2 - 2q_1\right)\gamma - 4s_1q_2\right)\Omega_0^2 + 8(s_2 + (\gamma/2))\xi\Omega_0$$

References

[1] Bathe KJ. Finite element procedures, 2nd ed. Watertown, MA; 2016. <http://meche.mit.edu/people/faculty/kjb@mit.edu> [also published by Higher Education Press China].
[2] Collatz L. The numerical treatment of differential equations. 3rd ed. Springer-Verlag; 1966.
[3] Noh G, Bathe KJ. An explicit time integration scheme for the analysis of wave propagations. Comput Struct 2013;129:178–93.
[4] Soares D. A novel family of explicit time marching techniques for structural dynamics and wave propagation models. Comput Methods Appl Mech Eng 2016;311:838–55.
[5] Kwon S-B, Lee J-M. A non-oscillatory time integration method for numerical simulation of stress wave propagations. Comput Struct 2017;192:248–68.
[6] Kim W, Lee JH. An improved explicit time integration method for linear and nonlinear structural dynamics. Comput Struct 2018;206:42–53.
[7] Newmark NM. A method of computation for structural dynamics. J Eng Mech Div (ASCE) 1959;85:67–94.
[8] Houbolt JC. A recurrence matrix solution for the dynamic response of aircraft. J Aeronaut Sci 1950;17:540–50.
[9] Wilson EL, Farhoomand I, Bathe KJ. Nonlinear dynamic analysis of complex structures. Int J Earthq Eng Struct Dyn 1973;1:241–52.
[10] Bathe KJ, Wilson EL. Stability and accuracy analysis of direct integration methods. Int J Earthq Eng Struct Dyn 1973;1:283–91.
[11] Zhou X, Tamma KK. Design, analysis, and synthesis of generalized single step single solve and optimal algorithms for structural dynamics. Int J Numer Meth Eng 2004;59:597–668.
[12] Shao HP, Cai CW. A three parameters algorithm for numerical integration of structural dynamic equations. Chin J Appl Mech 1988;5(4):76–81 (in Chinese).
[13] Shao HP, Cai CW. The direct integration three-parameters optimal schemes for structural dynamics. Proceedings of the international conference: machine dynamics and engineering applications. Xi'an Jiaotong University Press; 1988. C16–20.
[14] Chung J, Hulbert GM. A time integration algorithm for structural dynamics with improved numerical dissipation: the generalized-alpha method. J Appl Mech (ASME) 1993;60:371–5.
[15] Bathe KJ, Baig MMI. On a composite implicit time integration procedure for nonlinear dynamics. Comput Struct 2005;83:2513–24.
[16] Bathe KJ. Conserving energy and momentum in nonlinear dynamics: a simple implicit time integration scheme. Comput Struct 2007;85:437–45.
[17] Kroyer R, Nilsson K, Bathe KJ. Advances in direct time integration schemes for dynamic analysis. Automotive CAE Companion 2016;2016(2017):32–5.
[18] Zhang J, Liu Y, Liu D. Accuracy of a composite implicit time integration scheme for structural dynamics. Int J Numer Meth Eng 2017;109:368–406.
[19] Bathe KJ, Noh G. Insight into an implicit time integration scheme for structural dynamics. Comput Struct 2012;98–99:1–6.
[20] Noh G, Bathe KJ. Further insights into an implicit time integration scheme for structural dynamics. Comput Struct 2018;202:15–24.
[21] Wen WB, Wei K, Lei HS, Duan SY, Fang DN. A novel sub-step composite implicit time integration scheme for structural dynamics. Comput Struct 2017;182:176–86.
[22] Kim W, Choi SY. An improved implicit time integration algorithm: the generalized composite time integration algorithm. Comput Struct 2018;196:341–54.
[23] Malakiyeh MM, Shojaee S, Bathe KJ. The Bathe time integration method revisited for prescribing desired numerical dissipation. Comput Struct 2018. <https://doi.org/10.1016/j.compstruc.2018.10.008>.
[24] Benítez JM, Montáns FJ. The value of numerical amplification matrices in time integration methods. Comput Struct 2013;128:243–50.
[25] Graff KF. Wave motion in elastic solids. Oxford University Press; 1975.
[26] Noh G, Ham S, Bathe KJ. Performance of an implicit time integration scheme in the analysis of wave propagations. Comput Struct 2013;123:93–105.
[27] Kim KT, Zhang L, Bathe KJ. Transient implicit wave propagation dynamics with overlapping finite elements. Comput Struct 2018;199:18–33.